THE JOURNAL OF BIOLOGICAL CHEMISTRY VOL. 287, NO. 49, pp. 41406–41416, November 30, 2012

Identification of Amino Acid Residues Responsible for the Selectivity of Tadalafil Binding to Two Closely Related Phosphodiesterases, PDE5 and PDE6*[S]

Received for publication, June 6, 2012, and in revised form, October 1, 2012 Published, JBC Papers in Press, October 2, 2012, DOI 10.1074/jbc.M112.389189

Karyn B. Cahill[‡], Jonathan H. Quade[‡], Karen L. Carleton[§], and Rick H. Cote[‡1]

From the [‡]Department of Molecular, Cellular and Biomedical Sciences University of New Hampshire, Durham, New Hampshire 03824 and the [§]Department of Biology University of Maryland, College Park, Maryland 20742

Background: Most PDE5-selective inhibitors also potently inhibit photoreceptor PDE6.
Results: Evolutionary trace analysis predicted amino acids responsible for the selectivity of tadalafil binding to the PDE6 catalytic site without altering vardenafil binding.
Conclusion: A limited number of amino acid residues account for drug selectivity of PDE inhibitors.
Significance: This work will help identify more selective PDE5 inhibitors lacking adverse side effects on vision.

The 11 families of the Class I cyclic nucleotide phosphodiesterases (PDEs) are critical for regulation of cyclic nucleotide signaling. PDE5 (important in regulating vascular smooth muscle contraction) and PDE6 (responsible for regulating visual transduction in vertebrate photoreceptors) are structurally similar but have several functional differences whose structural basis is poorly understood. Using evolutionary trace analysis and structural homology modeling in conjunction with site-directed mutagenesis, we have tested the hypothesis that class-specific differences between PDE5 and PDE6 account for the biochemical and pharmacological differences in the two enzyme families. Replacing human PDE5 residues in the M-loop region of the binding site for the PDE5-selective inhibitor tadalafil (Cialis®) with the corresponding class-specific cone PDE6 residues (P773E, I778V, E780L, F787W, E796V, D803P, L804M, N806D, I813L, S815K) reduces tadalafil binding affinity to levels characteristic of PDE6. These mutations fail to alter vardenafil (Levitra®) affinity for the active site. Class-specific differences in PDE5 *versus* cone PDE6 that contribute to the accelerated catalytic efficiency of PDE6 were identified but required heterologous expression of full-length PDE5 constructs. Introduction of PDE6 residues into the background of the PDE5 protein sequence often led to loss of catalytic activity and reduced protein solubility, supporting the idea that multiple structural elements of PDE6 are highly susceptible to misfolding during heterologous expression. This work validates the use of PDE5 as a template to identify functional differences between PDE5 and PDE6 that will accelerate efforts to develop the next generation of PDE5-selective inhibitors with fewer adverse side effects resulting from PDE6 inhibition.

Changes in the intracellular concentration of cAMP and cGMP are responsible for a multitude of signaling pathways within eukaryotic cells. Regulation of these cyclic nucleotides can be achieved through a degradation mechanism utilizing one of the 11 family members of the Class I cyclic nucleotide phosphodiesterase (PDE)[2] superfamily (1). Two of the most thoroughly studied members of this PDE superfamily are the cGMP-specific photoreceptor PDE (PDE6) and a cGMP-specific PDE (PDE5) that is abundant in vascular smooth muscle and is the therapeutic target of drugs approved for the treatment of male erectile dysfunction and pulmonary hypertension.

The PDE6 family is unique in several respects: localization primarily to retinal photoreceptor cells, membrane anchoring by prenylation of the catalytic subunits, a distinct γ-subunit that regulates catalysis, enzyme activation mediated by a heterotrimeric G-protein, and diffusion-limited catalytic rate once activated (2). PDE6 is most closely related to PDE5 in its biochemical, structural, and pharmacological properties (3). Both PDE5 and PDE6 have highly conserved amino acid sequences and molecular organization (4–6). Of particular note, many PDE5 inhibitors, including Viagra® (sildenafil) and Levitra® (vardenafil), are either more potent or equipotent in inhibiting PDE6 catalysis (7–9); this lack of pharmacological selectivity by this group of compounds may account for the visual disturbances that are known to occur in humans taking these medications (10). In contrast, tadalafil (Cialis®) exhibits >200-fold selectivity for PDE5 over PDE6 and is not associated with visual disturbances. Intriguingly, mutations in PDE6 known to cause retinal degeneration (RetNet) are located in areas of very high sequence similarity with PDE5, although at present no genetic diseases linked to PDE5 defects have been reported.

Despite many similarities, PDE5 and PDE6 differ in several important ways. First, the ability of individual PDE5 inhibitors

* This work was supported, in whole or in part, by National Institutes of Health Grant R01 EY05798-24 (to R. H. C.) Partial funding was provided by the New Hampshire Agricultural Experiment Station; this is Scientific Contribution Number 2482.
[S] This article contains supplemental Table S1 and Fig. S1.
[1] To whom correspondence should be addressed: Dept. of Molecular, Cellular, and Biomedical Sciences, University of New Hampshire, 46 College Rd., Durham, NH 03824. Tel.: 603-862-2458; Fax: 603-862-4013; E-mail: rick.cote@unh.edu.

[2] The abbreviations used are: PDE, phosphodiesterase; PDE6, photoreceptor PDE; PDE5, the cGMP-specific PDE abundant in vascular smooth muscle; GAF, a protein domain named for some of the proteins in which it is found, including cGMP binding phosphodiesterases, adenylyl cyclases, and the bacterial FhlA protein; GAFa and GAFb, first and second GAF domains arranged in tandem in GAF-containing PDEs; CD, catalytic domain; aa, amino acids.

(*e.g.* Cialis®/tadalafil) to preferentially bind to the PDE5 over the PDE6 active site implies structural differences in the catalytic pocket that have not been elucidated but have therapeutic implications. Second, the catalytic mechanism of cGMP hydrolysis by PDE6 operates 500-fold faster than for PDE5. Although two residues in bovine PDE5 (Ala-608 and Ala-612) when mutated to their PDE6 counterparts (glycine) increase the turnover rate of cGMP ~10-fold (11), the structural basis for PDE6 to catalyze cGMP hydrolysis at the diffusion-controlled limit is not known. Third, whereas recombinant expression of full-length PDE5 is routinely accomplished in eukaryotic cells with properties very similar to the native enzyme (12), PDE6 catalytic subunits cannot be heterologously expressed in a soluble and active state in biochemical quantities (13–17); successful ectopic expression of cone PDE6 in transgenic frogs is a notable exception, but protein yields are low (18). Finally, PDE5 does not use a separate regulatory protein analogous to the Pγ subunit but rather is allosterically regulated by cGMP binding to noncatalytic sites and by phosphorylation (19).

Identification of the amino acid residues in the drug binding pocket responsible for the reduced affinity of tadalafil for PDE6 compared with PDE5 is of great importance for the development of new PDE5 inhibitors with greater selectivity for PDE5 and, hence, fewer potential adverse side effects (20–22). Efforts to identify the critical pharmacophores using drug discovery approaches have shown limited success (23, 24). The challenge for developing drugs that discriminate PDE5 from PDE6 is highlighted by the fact that 7 of the 11 residues known to interact with tadalafil are also observed to interact with vardenafil (25). Other structural and site-directed mutagenesis studies support the idea that a relatively small number of residues are responsible for the selectivity of tadalafil for PDE5 over PDE6 (12, 26). It should be noted that efforts to understand PDE5/PDE6 drug selectivity are also relevant to other PDE families (*e.g.* tadalafil exhibits poor selectivity for PDE5 *versus* PDE11 (20)).

Examination of several different PDE5 crystal structures with the same ligand bound shows excellent agreement regarding interacting amino acids in the core of the drug binding pocket, whereas there is a lack of consensus on the secondary structures of more disordered elements designated as the H- and M-loops (26–28). For these reasons more knowledge about the residues involved in these drug/enzyme interactions is needed to develop new PDE inhibitors with greater specificity and fewer side effects.

We have taken advantage of the structural information available on PDE5 along with the extensive sequence data for both PDE5 and PDE6 families to identify sites with a high probability of conferring functional differences (*e.g.* drug discrimination, catalytic efficiency). For this purpose, we employed evolutionary trace analysis (29, 30) that is based on the idea that amino acid residues that are highly conserved throughout evolution are most likely to be of functional significance. By first performing a multiple sequence alignment of the closely related PDE5 and PDE6 families using sequences from evolutionarily distant species, we identified "unanimous" residues (identical throughout all PDE5 and PDE6 sequences) and "class-specific" residues (100% conserved in all PDE5 sequences and a different, but 100% conserved, residue in all PDE6 sequences).

We then homology-modeled the human PDE6C sequence onto the crystal structures of the human PDE5 catalytic domain (crystal structures of the PDE6 catalytic domain are not currently available nor are full-length PDE5 structures) to assist in the identification of plausible residues based on orientation to the catalytic pocket and proximity to known ligand binding sites. By converting residues in PDE5 to their class-specific PDE6 counterparts using site-directed mutagenesis, we have identified the critical amino acids within the drug binding pocket that contribute to the selectivity of tadalafil for PDE5 relative to PDE6. We also examined some of the sites that might contribute to differences in catalytic properties and the ability to express recombinant protein as PDE5 residues are changed into their PDE6 counterparts.

EXPERIMENTAL PROCEDURES

Materials—Restriction enzymes, calf intestine phosphatase, and T4 DNA ligase were purchased from New England Biolabs. The AccuScript High Fidelity RT-PCR system, Pfu Ultra II DNA polymerase, and the QuikChange and QuikChange Lightning Multi-site-directed mutagenesis kits were from Agilent Technologies. All initial cloning of pcDNA3, pFastBac Htb dual, pGEX-4T-1, and pGEX-6P-1 vectors were performed in Max efficiency DH5α-T1^R-competent cells (Invitrogen). RNA isolation and plasmid purification kits were from Qiagen. All tissue culture reagents, PCR SuperMix, and oligonucleotides were purchased from Invitrogen. Lysonase, Rosetta-competent cells, and Ni^{2+}-nitriloacetic acid-agarose were obtained from EMD Biosciences. [^{3}H]cGMP was from GE HealthCare and PerkinElmer Life Sciences. Immobilized glutathione-agarose was from Thermo Fisher. Fetal bovine serum, the complete open reading frame for human PDE5, vardenafil, and tadalafil were gifts provided by Bayer Healthcare AG. All other reagents were from Sigma.

Collection of PDE5 and PDE6 Protein Sequences and Evolutionary Trace Analysis—Full-length PDE5 and PDE6 vertebrate sequences (see supplemental Fig. S1) were obtained from NCBI, the Sanger Institute, the Joint Genome Institute, and Genoscope as well from our own independent cDNA sequencing. Predicted protein sequences from genomic DNA sequencing projects were individually analyzed to determine intron/exon boundaries; only those sequences that were full-length were included in our analysis. Sequences were initially aligned using ClustalW and manually adjusted as needed. A phylogenetic tree was constructed from this alignment (supplemental Fig. S1) and tested using PAUP (31). Saturated evolutionary trace analysis was carried out as described in detail in Ref. 29 to verify that a sufficient number of phylogenetically diverse sequences had been collected (Fig. 1).

Homology Modeling—Based on the sequence alignment for PDE5 and PDE6 sequences described above (a portion of which is shown in Fig. 2), we used SWISS-MODEL (32) to perform structural homology modeling of the human PDE6C catalytic domain structure based on three different PDE5 crystal structures available in the Protein Data Bank: PDB code 1T9S (complexed with GMP (33)), PDB code 1XOZ (complexed with tada-

TABLE 1

Site-directed mutants of PDE5 and their catalytic properties

Numbering refers to the human PDE5 sequence with single-letter amino acid abbreviations for site-directed mutations. PDE5WT and its mutants are full-length recombinant proteins expressed in insect cells. The isolated CD and its mutants were expressed in bacteria. cGMP hydrolytic activity (turnover number, k_{cat}, and Michaelis constant (K_m) with cGMP as substrate) was measured using a radiotracer assay (2–10 nM PDE5 and 50 μM cGMP). Drug inhibition constants (K_i) were determined using 0.5 nM enzyme and 240 nM [^{3}H]cGMP. The values for k_{cat} and K_i represent the mean ± S.E. ($n \geq 3$); values without S.E. are from one determination. K_m values are the average of at least 2 independent experiments (<20% variation). Kinetic parameters for the wild-type enzyme are within the range reported in the literature, whereas the K_i value for vardenafil under our experimental conditions was ~10-fold higher (see "Experimental Procedures") than previously reported (41).

Construct	PDE5 to PDE6C residues	$k_{cat\ (cGMP/s/PDE)}$	K_m	K_i	
				Vardenafil	Tadalafil
			μM	nM	nM
PDE5WT		1.5 ± 0.2	2.4	2.3 ± 0.8	1.9 ± 0.2
PDE5m1	A618G, T621V, A622G	9.6 ± 0.8	5.2	1.0 ± 0.2	2.8 ± 1.1
PDE5m2	A618G, T621V, A622G, F686L	3.4 ± 0.3	ND	1.0	4.0 ± 2.8
PDE5m4	P773E, I778V, E780L	1.5 ± 0.2	2.7	2.0	7.6 ± 1.1
PDE5m5	D803P, L804M, N806D	1.2 ± 0.2	3.9	0.9	7.4 ± 2.5
PDE5m6	P773E, I778V, E780L, D803P, L804M, N806D	0.6 ± 0.1	ND	0.8 ± 0.2	27.0 ± 2.5
CD/WT		1.6 ± 0.3	2.5	3.0 ± 1.1	2.0 ± 0.7
CD/m6	P773E, I778V, E780L, D803P, L804M, N806D	1.2 ± 0.1	4.6	2.4 ± 1.4	50.3 ± 10.0
CD/m6.1	P773E, I778V, E780L, D803P, L804M, N806D, F787W, E796V	2.6 ± 0.4	ND	0.6	12.1 ± 1.5
CD/m6.2	P773E, I778V, E780L, D803P, L804M, N806D, I813L, S815K	1.8 ± 0.3	5.5	1.25	164 ± 35
CD/m7	P773E, I778V, E780L, D803P, L804M, N806D, F787W, E796V, I813L, S815K	7.5 ± 1.3	3.0	3.1 ± 0.3	210 ± 42

lafil (25)), and PDB code 1XPO (complexed with vardenafil (25)). These models were visualized using PyMOL Version 1.3 (Schrödinger, LLC). Assessment of the quality of the homology model was determined by a Ramachandran plot and analyzed with ProCheck (34).

Cloning of the Human Full-length PDE5 Wild-type (wt) and Mutant Constructs—The pFastBac vector was modified by replacing the tobacco etch virus sequence with a His_6 tag sequence and the HRV3C protease cleavage site downstream of the polyhedrin promoter. In addition, the open reading frame for the enhanced GFP sequence was cloned downstream of the p10 promoter to use as a transfection indicator. All full-length constructs were cloned into the vector at the EcoRI and NotI restriction sites. All amplifying or mutagenizing oligonucleotide sequences were verified. Human *PDE5* wt DNA (NP_001074) was amplified in a one-step PCR reaction using 50 ng of DNA template and 200 ng of each primer. Complementary oligonucleotide pairs containing the base changes needed to generate the PDE5 to PDE6 mutations were added to PCR reactions with pFastBac PDE5 DNA as the template; the manufacturer's protocol for the QuikChange site-directed mutagenesis kit was used. Mutants PDE5m2, -m4, and -m6 were constructed using two subsequent mutagenesis reactions, the later reaction using a former one as a template. All mutants listed in Table 1 were verified to consist of the correct sequence by automated DNA sequencing using an ABI3130 genetic analyzer and BigDye Terminator reagents at the Hubbard Center for Genomic Studies Sequencing Center (University of New Hampshire).

Cloning of the Human PDE5 Catalytic Domain (CD), GAF Catalytic Domains (GAFb and GAFab), and Mutant Constructs—All catalytic domain constructs (consisting of aa 503–875 of human PDE5) were cloned into the pGEX-4T vector at the SmaI and NotI restriction sites. Longer constructs consisting of the catalytic domain plus the GAFb (aa 332–875) or GAFa-GAFb (aa 81–875) domains were cloned into pGEX-6P at the EcoRI and NotI restriction sites. The PDE5 wt catalytic domain (CD/wt) was generated by cloning an 1130 nucleotide BamHI (filled in) to NotI fragment from the full-length PDE5 wt directly into a SmaI-NotI-linearized pGEX-4T vector. PDE5 GAFb-catalytic domain construct (GAFb/wt) was generated by a PCR reaction using PDE5 wt as a template. The GAFb/m1 mutant was made by replacing the NcoI-NotI fragment in GAFb/wt with an identical fragment from the full-length PDE5m1 containing the m1 mutation. The GAFab/wt construct was generated using a 3′ primer that binds within the GAFb region of PDE5 where a HindIII restriction site exists. This PCR product, which generated EcoRI-HindIII ends, was directly cloned into linearized pGEX+ GAFb/wt where the GAFb region was replaced with the longer GAFa-GAFb sequence. The GAFab/m1 was constructed by removing the HindIII-NotI catalytic domain fragment from pGEX+ GAFab/wt and replacing it with the identical fragment from pGEX+GAFb/m1 containing the m1 grouping of three mutated residues. Finally, we also constructed human full-length PDE6C (CAA64079) into the modified pFastBac vector and several human PDE6C catalytic domains (aa 432–819, 432–858, 503–819, and 503–858) into the pGEX-4T vector, all of which failed to express soluble, active protein.

Baculovirus Generation, Protein Expression, and Affinity Purification of Recombinant Full-length PDE5 wt and Mutant Constructs—Bacmid DNAs were generated by transforming competent DH10Bac cells using the manufacturer's Bac-to-Bac protocol. Adherent Sf9 cells were transfected with a mixture of 5 μg of purified bacmid clones and 20 μl of SuperFect and incubated at room temperature for 4–5 h. DNA-dendrimer complex was removed and replaced with media containing 10% FBS and incubated at 27 °C for 90–120 h. Cells were harvested, and the virus-containing supernatant was used in a viral plaque assay to obtain individual viral isolates to screen for protein expression. Harvested cells were analyzed by immunoblotting to test for His-tagged PDE5 expression. Viral supernatants from positive cells were used to generate high titer viral stocks for subsequent large scale infections.

Suspension cultures of Sf9 cells grown in SF900II with 2% FBS were infected at a multiplicity of infection of 5 plaque forming units/ml for 48–60 h at 27 °C. Harvested cells (~1 g) were lysed in 8 ml of cold 20 mM Tris, pH 8, 100 mM NaCl, and 100 μl of Sigma protease inhibitor mixture without EDTA. The cell suspension was sonicated for ten 20-s pulses on ice with 40-s

intervals between sonications. The suspension was centrifuged, and the soluble supernatant was loaded onto a 2.5-ml Ni^{2+}-nitriloacetic acid-agarose column equilibrated with lysis buffer. The remaining purification followed the manufacturer's protocol with the addition of 25 mM imidazole in the wash buffer and 250 mM imidazole in the elution buffer. Fractions containing cGMP hydrolytic activity were pooled, and the protein was immediately buffer exchanged into 20 mM Tris pH 7.5, 100 mM NaCl, 2 mM $MgCl_2$, and 2 mM DTT and concentrated using an Amicon 15 Ultra 30,000 molecular weight cutoff. Glycerol was added to a final concentration of 45% w/v, and purified protein was stored at −20 °C. Hydrolytic activity was maintained for several months of storage, but cGMP-induced changes in drug binding affinity (35) were not observed in these preparations, probably as a result of the effects of long term storage on PDE5 regulatory properties (36). Typical yields were 1–3 mg of recombinant protein per liter.

Bacterial Expression and Protein Purification of Recombinant PDE5 CD Constructs—pGEX constructs were transformed into the Rosetta strain of *Escherichia coli* BL21(DE3) competent cells. Single colony isolates were grown in 1 liter of LB medium containing ampicillin and chloramphenicol at 37 °C until the cells reached an A_{600} of 0.8–1. The cells were induced with 0.2 mM isopropylthiogalactoside and incubated at 15 °C for 24 h. Cell pellets were resuspended in 30 ml of cold 50 mM Tris, pH 8, 200 mM NaCl, 5 mM DTT, lysonase reagent, and bacterial protease inhibitor. The cell suspension was sonicated for forty 20-s pulses on ice with 40-s intervals between sonications. The suspension was centrifuged, and the soluble supernatant was loaded onto an immobilized glutathione agarose column (1.5-ml packed resin) equilibrated with lysis buffer. The manufacturer's purification protocol was followed except that 5 mM reduced glutathione was added to the elution buffer. Peak fractions were immediately pooled and buffer-exchanged into 20 mM Tris, pH 7.5, 100 mM NaCl, 2 mM $MgCl_2$, and 2 mM DTT to minimize exposure to glutathione. Glycerol was added to 45% w/v. Purified proteins were stored at −20 °C.

Protein and Enzyme Assays—Protein concentrations were determined by the method of Bradford (37). Purity was assessed by quantifying band intensity on Coomassie-stained gels. Purity of PDE5 recombinant proteins after affinity purification was typically 70–90%, with the exception of CD/m1 (~50%). PDE5 catalytic activity was measured using a radiotracer assay (38). Pharmacological studies of the inhibition by vardenafil and tadalafil were conducted at an enzyme concentration of 0.5 nM using 240 nM total cGMP.

Data Analysis—Except where noted, experiments were repeated at least 3 times, and average values were reported as the mean ± S.E. Curve fitting was performed with SigmaPlot (SPSS, Inc., Chicago, IL). The IC_{50} for drug inhibition was determined by fitting the experimental data to a three-parameter logistic dose-response function. K_i values were determined using the equation $K_i = IC_{50}/(1 + [cGMP]/K_m)$.

In Silico Docking of Ligand to the Binding Pocket—To predict the orientation and contact sites of tadalafil or vardenafil within the catalytic domain of the homology models for PDE5, PDE6, or the mutants created for this study, we docked the drug to the enzyme active site using AutoDock/Vina (39). We used the solved crystal structures for PDE5 catalytic domain with tadalafil (PDB code 1XOZ) or vardenafil (PDB code 1XP0) to validate the accuracy of the docking algorithm (25). The imported ligand files for both tadalafil and vardenafil contained one and eight, respectively, rotatable bonds; Gasteiger charges and nonpolar hydrogens were added. The torsion root atom (C9 for vardenafil, C13 for tadalafil) was also chosen. To the protein structure file for the unliganded PDE5 catalytic domain, polar hydrogens were added, missing atoms were corrected, and atomic Gasteiger charges were calculated and added. Using the GridBox option, the three-dimensional parameters for docking the ligand to the protein were determined; for tadalafil, the grid center coordinates were $x = 48.75$, $y = 37.45$, and $z = 16.5$, and the size coordinates were $x = 30$, $y = 16$, and $z = 20$; for vardenafil, the grid center coordinates were $x = -25.55$, $y = 26.55$, and $z = 60.35$, and the size coordinates were $x = 16$, $y = 16$, and $z = 18$. The docked ligand output file was viewed, and atomic distances and interactions were analyzed using PyMOL.

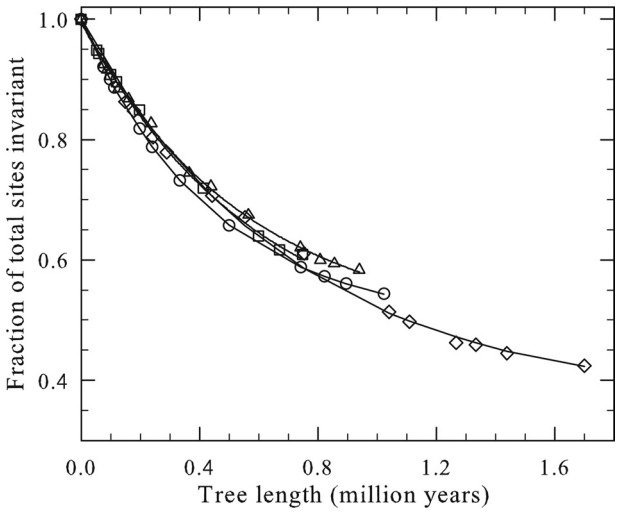

FIGURE 1. **Saturated evolutionary trace analysis of PDE5 and PDE6 sequences.** Protein sequences from PDE5 (○, 13 sequences), rod PDE6A (□, 10 sequences), rod PDE6B (△, 13 sequences), and cone PDE6C (◇, 14 sequences) were aligned, and phylogenetic analysis conducted using PAUP (see "Experimental Procedures"). The curves represent the fit of the data to the saturation equation (% saturation = $(1 - f_a)/(1 - f_s) \times 100$; see "Experimental Procedures") where *fa* is the actual fraction of invariant sites, and *fs* is the predicted fraction at saturation (infinite time). Based on these fits, the percent saturation of each gene is: PDE5, 90%; PDE6A, 73%; PDE6B, 83%; PDE6C, 91%.

RESULTS AND DISCUSSION

Use of Evolutionary Trace Analysis to Identify Differences between PDE5 and PDE6—We first collected an evolutionarily diverse set of sequences of vertebrate *PDE5* and the two rod (*PDE6A* and *PDE6B*) and one cone (*PDE6C*) genes. A multiple sequence alignment of these 50 full-length sequences was performed followed by construction of a phylogenetic tree (supplemental Fig. S1). Based on this phylogenetic analysis, we then used saturation analysis (29) to evaluate whether a sufficient number of phylogenetically diverse sequences had been collected to accurately categorize variable and invariable amino acid residues. As shown in Fig. 1, *PDE5* and *PDE6C* had achieved ~90% saturation, whereas the rod genes were somewhat lower (*PDE6A* = 73%, *PDE6B* = 83%). For the purpose of

TABLE 2

Identification of highly conserved regions of the PDE5 and PDE6 amino acid sequences

Fifty PDE5 and PDE6 amino acid sequences were compiled, aligned, and analyzed as described under "*Experimental Procedures.*" Human PDE5 and PDE6C were used as the reference sequences for numbering purposes. The boundaries of each region were chosen based on current information from x-ray crystallographic results for the PDE5 GAFa-GAFb structure (PDB codes 3MF0 and 3LFV) and the catalytic domain (PDB codes 1XOZ and 1XP0). The diagram identifies the regions based on the human PDE5 sequence: G, gap between GAFa and GAFb: L, linker region between GAFb and catalytic domain; H, H-loop structural element; M, M-loop structural element: dotted and solid vertical lines represent sites mutated to test catalytic activity and drug binding, respectively.

The occurrence of unanimous and class-specific sites overall and within each defined region was determined using saturated evolutionary trace analysis. For the catalytic domain, 35 class-specific residues were identified at the following PDE5 sites: Asp-568, Thr-571, Asp-581, Ala-618, Thr-621, Leu-646, Leu-655, Val-660, Ser-663, Ile-665, Arg-667, Tyr-676, Phe-686, Leu-690, Gln-699, Lys-714, Leu-721, Phe-736, Leu-759, Pro-773, Ile-778, Glu-780, Phe-787, Glu-796, Asp-803, Leu-804, Asn-806, *Ile-813*, Ser-815, Ala-823, Leu-828, Leu-832, Ser-836, Cys-839, Leu-842; underlined and italicized residues represent drug interaction sites for tadalafil and vardenafil, respectively, based on their crystal structures.

In addition, the sites within the PDE5 or PDE6 family that did not meet the criteria for evolutionary trace analysis but that were 100% conserved within the gene family are tabulated as PDE5 invariant or PDE6 invariant. Regions of percent invariance that exceed 50% within a given gene are indicated in *boldface*.

	Total # of amino acids	N-terminal region	GAFa domain	gap	GAFb domain	linker region	Catalytic domain	C-terminal region
PDE5	875	1-163	164-316	317-342	343-498	499-533	534-861	862-875
PDE6C	858	1-72	73-226	227-252	253-428	429-483	484-820	821-858
PDE5 region size (a.a.)		163	152	25	155	34	327	13
PDE6 region size (a.a.)		72	153	25	175	54	336	37
Unanimous sites	118	0	12	1	21	2	82	0
Class-specific sites	72	1	8	2	21	5	35	0
PDE5 invariant sites	278	32	**87**	**17**	30	**24**	86	2
PDE6 invariant sites	99	3	6	4	50	1	35	2
PDE6A invariant sites	321	20	47	**16**	**93**	18	124	3
PDE6B invariant sites	304	12	47	**17**	**90**	24	108	6
PDE6Cinvariant sites	168	7	15	5	67	6	63	5

comparing PDE5/PDE6 differences, we grouped the three PDE6 sequences together and concluded that for both PDE5 and the grouped PDE6 sequences, we were likely to have correctly identified at least 90% of the conserved sites as being invariant during vertebrate evolution (29).

Table 2 provides a summary of the results of this evolutionary trace analysis. When the entire amino acid sequence is considered, 118 amino acids (13%) are the same amino acid residue among all 50 PDE5 and PDE6 sequences. Nearly 70% of these unanimous sites are found within the catalytic domain (representing ~25% of the total amino acids in this domain). This high extent of unanimity within the catalytic domain is not surprising in that all 11 PDE families share a number of invariant sites that reflect the structural and enzymatic elements required by all Class I cyclic nucleotide phosphodiesterases (Pfam domain name: PDEase_I). The high degree of overall sequence similarity within the catalytic domain highlights the challenge in using sequence information to infer functional differences that can translate into synthesizing the next generation of PDE5 inhibitors with greater target selectivity.

We identified 72 amino acids (8%) in PDE5 and PDE6 that met the criteria for being classified as class-specific sites, of which 21 sites reside in the GAFb domain and 35 sites are located in the catalytic domain (Table 2). Of the 35 class-specific sites in the catalytic domain, only 10 are found within 10 Å of the drug binding site (as determined by the crystal structures of PDE5 catalytic domains with bound ligands (25, 26, 33, 40)). We hypothesize that these 10 class-specific sites may account for the pharmacological differences that distinguish the PDE5 and PDE6 enzyme families. Likewise, some of the class-specific sites found in the regulatory, N-terminal half of the protein sequence may reflect a divergence of the allosteric regulatory mechanisms employed by these two enzyme families (see the Introduction).

We also examined sites that were invariant throughout vertebrate evolution of one PDE gene but failed to meet the more stringent criterion of being class-specific sites (Table 2). We found that PDE5 had ~3-fold more invariant sites than the PDE6 family. However, when the rod and cone sequences were analyzed individually, PDE6A and PDE6B were found to have a

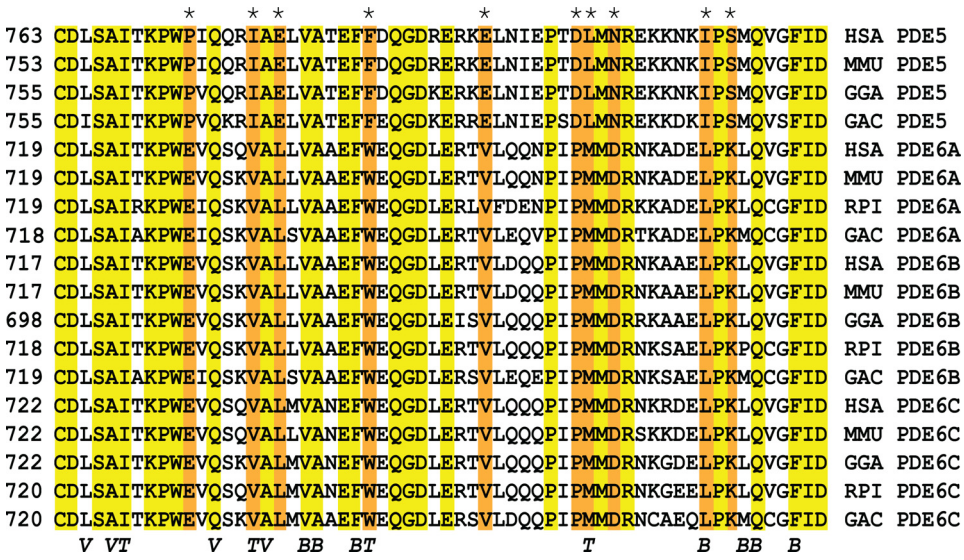

FIGURE 2. **Sequence alignment for the drug binding region of the catalytic domain.** A multiple sequence alignment of the region (aa 763–822 of the human PDE5 sequence) representing the core of the drug binding pocket is shown for a selected number of evolutionarily diverse species (but that applies for the entire 50 sequences that were used in the evolutionary trace analysis). Species abbreviations are the same as in supplemental Fig. S1. *Asterisks* (*) denote sites that were mutated in this study. *Yellow* represents unanimous sites, and *orange* indicates class-specific sites. Beneath the alignment, the *letters* indicate sites of interaction of vardenafil (*V*), tadalafil (*T*), or both (*B*) with the drug binding pocket, as determined in the x-ray crystal structures (25); for clarity, two additional vardenafil contact residues (Leu-725 and Trp-853) outside this region are not included in the alignment.

similar number of invariant sites as PDE5, whereas PDE6C sequences are more variable. Invariant sites exist in clusters, particularly in the regulatory domains of the protein. The PDE5 GAFa domain, the adjoining gap region between GAFa and GAFb, and the region that links GAFb to the catalytic domain (but not the GAFb domain itself) all contain 60–70% invariant sites. In contrast, the two rod PDE6 genes showed the greatest number of invariant sites (93 sites for PDE6A and 90 sites for PDE6B; ~50%) in the GAFa-GAFb gap region and within the GAFb domain. The localization of class-specific and invariant residues to different regulatory regions of PDE5 and PDE6 most likely reflect the different mechanisms of enzyme regulation; that is, direct allosteric activation by cGMP binding to GAFa in the case of PDE5 and multiple sites of interaction of the inhibitory γ-subunit of PDE6 with the PDE6 GAF domains. When comparing invariant sites within the PDE6 family, it is notable that rod PDE6A and PDE6B genes have undergone many fewer amino acid substitutions than cone PDE6C during evolution, suggesting a greater selective pressure on rod PDE6 to retain its primary amino acid sequence.

In summary, multiple sequence alignment of an evolutionarily diverse set of PDE5 and PDE6 sequences has identified discrete, highly conserved regions, including the catalytic domain and the GAFa and GAFb regulatory domains that likely reflect functionally significant differences in the regulation of PDE families. We focus attention below on class-specific sites located within the catalytic pocket, adjacent α-helices, and the H- and M-loop regions that are likely to be important interaction sites with PDE inhibitors and with substrates.

Identification of Amino Acid Residues That Distinguish PDE5 and PDE6 Drug Selectivity—The PDE5-selective inhibitors sildenafil and vardenafil also potently inhibit the photoreceptor PDE6 enzymes. In contrast, the PDE5-selective inhibitor tadalafil is unique among the commercially available PDE5 inhibitors in having a 210-fold lower affinity for PDE6 than for PDE5 (9). The molecular basis for this difference in tadalafil affinity for PDE5 and PDE6 is largely unknown but of great therapeutic significance.

To address the question of the molecular determinants of drug binding, we relied on the identification of class-specific sites from evolutionary trace analysis (Table 2) along with structural information available on the drug interaction sites for vardenafil and tadalafil (25). The sequence alignment and identification of residues involved in the drug binding region is shown in Fig. 2.

We next performed structural homology modeling (see "Experimental Procedures") of the human PDE6C catalytic domain based on the appropriate PDE5 crystal structures with bound drug. The stereochemical quality of the PDE6C structural homology model liganded with tadalafil was assessed, and we found that 92% of the PDE6C residues were located within the "most favored" regions determined by PROCHECK; the vardenafil PDE6C homology model gave a similarly good fit to the PDE5 template (data not shown).

The solved crystal structures for PDE5 bound to tadalafil or vardenafil (25, 26) have identified seven interaction sites that are shared in common by both drugs (identified as *B* at the *bottom of the alignment* in Fig. 2). Five of these seven shared sites are unanimous and were, therefore, ruled out as contributing to drug discrimination. Based on our evolutionary trace analysis and structural homology modeling results, 3 of the 10 class-specific sites in the defined drug binding region (Ile-778, Phe-787, Leu-804) were identified as the top candidates for discriminating tadalafil from vardenafil because they interact with tadalafil, but not vardenafil, in the PDE5 crystal structure. Two initial PDE5 mutants (Table 1) were created to each introduce three different class-specific amino acid replacements; PDE5m4 contained P773E, E780L, and one of the tadalafil-interacting residues (I778V), whereas PDE5m5 contained D803P, N806D, and another tadalafil-interacting site (L804M). A third

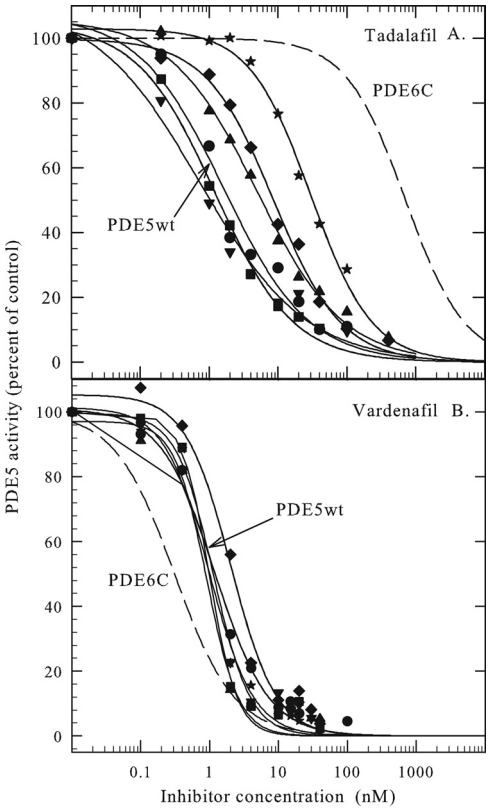

FIGURE 3. **Pharmacological properties of full-length PDE5 site-directed mutants.** Purified full-length His-tagged PDEs (500 pM) were preincubated with tadalafil (*A*) or vardenafil (*B*) for 20 min at room temperature followed by the addition of 240 nM [^{3}H]cGMP to measure catalytic activity. Plotted data are from one representative experiment testing wt (●) and the following PDE5 mutants: m1 (▼), m2 (■), m4 (♦), m5 (▲), m6 (★). The *dashed line* represents published data from our laboratory for cone PDE6 (9). The K_i value for tadalafil for PDE6C = 700 nM. The K_i value for vardenafil for PDE6C = 0.3 nM. The IC_{50} for each construct was obtained from curve-fitting the data to a logistic function and used to calculate the inhibition constant (see "Experimental Procedures"). The calculated K_i values are given in Table 1.

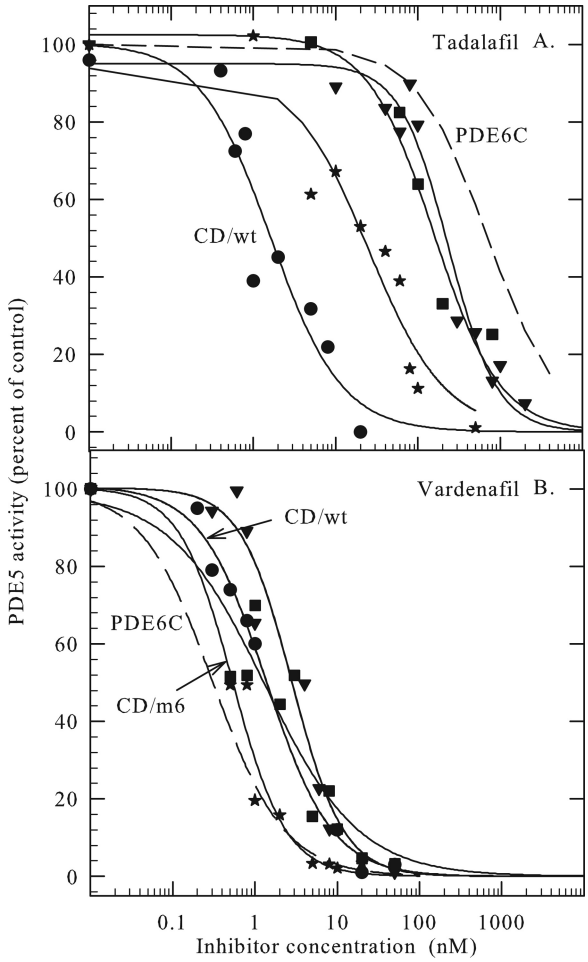

FIGURE 4. **Pharmacological properties of catalytic domain PDE5 site-directed mutants.** Purified GST-tagged PDE5 catalytic domains (500 pM) were preincubated with tadalafil (*A*) or vardenafil (*B*) for 20 min at room temperature followed by the addition of 240 nM [^{3}H]cGMP to measure catalytic activity. Plotted data are from one representative experiment testing wt (●), m6 (★), m7 (▼) and m6.2 (■) the *dashed line* is the literature value for cone PDE6C (9). The K_i value for tadalafil for PDE6C = 700 nM. The K_i value for vardenafil for PDE6C = 0.3 nM. The IC_{50} was determined as in Fig. 3, and the K_i values are given in Table 1.

mutant (PDE5m6) was created that incorporated all six of these amino acid substitutions. The mutants were constructed as N-terminal His-tagged proteins containing the complete PDE5 sequence and expressed in insect cell cultures. All recombinant proteins were expressed in a soluble form and displayed kinetic properties similar to the native PDE5 enzyme (Table 1).

Of the three full-length PDE5 constructs designed to disrupt tadalafil binding to the active site, PDE5m6 (P773E, I778V, E780L, D803P, L804M, and N806D) showed the greatest (15-fold) decrease in tadalafil inhibitory potency (Fig. 3*A*). The amino acid residues mutated in PDE5m6 are located in α-helix 14 and the adjoining M-loop, structural elements known to contribute to the substrate and inhibitor binding pocket. These same changes failed to significantly affect vardenafil binding (Fig. 3*B*). The individual triple mutants (PDE5m4 and PDE5m5) each showed a 3–5-fold reduction in tadalafil binding affinity (Fig. 3*A*), demonstrating that each set of mutations influenced drug binding.

To accelerate the creation of additional site-directed mutants, we expressed the isolated catalytic domain of PDE5 in *E. coli*. To improve recovery of soluble, purified protein, our constructs were created as N-terminal GST fusion proteins to amino acids 503–875 of the human PDE5 sequence. The wild-type PDE5 catalytic domain (CD/wt) expressed in bacteria had kinetic and pharmacological properties indistinguishable under our experimental conditions from the corresponding full-length protein expressed in insect cells (Table 1).

Using the bacterially expressed catalytic domain containing the six mutations in the PDE5m6 mutant (designated CD/m6), the four remaining class-specific sites in this region of the catalytic domain (F787W, E796V, I813L, S815K) were also introduced to create CD/m7. Residue Phe-787 is a known tadalafil-interacting site, whereas Ile-813 has been shown to interact with both vardenafil and tadalafil (25). Fig. 4*A* shows that the combination of all 10 mutations seen in CD/m7 reduced tadalafil affinity (K_i = 210 ± 42 nM) to a value within ~3-fold that of the value for cone PDE6 (K_i = 700 nM; (9)). Importantly, no significant disruption of interactions between vardenafil and the drug binding site was observed (Fig. 4*B*).

To refine our understanding of the individual sites responsible for tadalafil discrimination, we also created mutants in

which only 8 of the 10 class-specific residues were mutated (CD/m6.1 or CD/m6.2; Table 1). Whereas the CD/m6.1 mutant paradoxically showed a modest increase in tadalafil affinity compared with CD/m6, the CD/m6.2 mutant was observed to more closely mimic the CD/m7 mutant in terms of reduced affinity for tadalafil (Fig. 4*A*; Table 1). In summary, our results do not support the idea that only a few amino acid residues within the drug binding pocket of PDE6 are responsible for tadalafil discrimination. Instead, many of the 10 class-specific sites in the drug binding pocket incrementally contribute to disrupting the favorable interactions that occur in PDE5 but not in PDE6.

Molecular Simulation of Drug Binding to the PDE5 Catalytic Site—To better understand the consequences of these mutations on drug binding to the catalytic site, we performed *in silico* docking of both drugs to the mutants we had constructed as well as to the PDE6C catalytic domain using Autodock (see "Experimental Procedures"). We first established the accuracy of the docking procedure by comparing the *in silico* docking results to the published crystal structures of the PDE5 catalytic domains with either vardenafil or tadalafil bound. The docking results yielded only one possible conformation for the ligand that superimposed very well with the conformation of the ligand observed in the liganded crystal structures for both tadalafil (Fig. 5*A*) and vardenafil (Fig. 5*B*).

Fig. 6 demonstrates the dramatic shift in tadalafil binding to the catalytic site of PDE5 upon introduction of the 10 amino acid substitutions that convert the PDE5 wild-type catalytic domain into the CD/m7 mutant. Fig. 6*A* shows the conformation of tadalafil (*orange*) within the PDE5 catalytic domain in which the 10 class-specific sites in the vicinity of the drug are highlighted (*light brown*), including the four *ball-and-stick residues* that are observed to interact with tadalafil in the published crystal structure (25). These 10 residues are located in α-helix 14 (Pro-773, Ile-778, Glu-780, Phe-787, and Glu796), the adjoining M-loop (Asp-803, Leu-804, and Asn-806), and the initial residues of α-helix 15 (Ile-813 and Ser-815).

Upon converting these 10 PDE5 residues to their PDE6 counterparts (Fig. 6*B*, *green*), tadalafil (*yellow*) completely changes its orientation within the catalytic site, consistent with the 100-fold decrease in binding affinity. Overall, the docked conformation of tadalafil in the CD/m7 mutant shifts the drug closer to the cyclic nucleotide binding pocket and the metal ions of the PDE5 catalytic core. We speculate that several of the mutations may cumulatively account for this displacement of tadalafil from its original binding site; 1) the non-conservative S815K mutation disrupts four of the eight polar contacts present in the wild-type structure; 2) introduction of the sulfur atom in the L804M mutation may disrupt the hydrophobic interactions that existed between the leucine side chain and the methylenedioxyphenyl ring of tadalafil; 3) one or more mutations in the vicinity of Q817 may disrupt the hydrogen bond that exists between this residue and tadalafil in the wild-type structure (25); 4) five polar interactions are lost as a result of the D803P mutation that may adversely affect ligand binding; 5) the N806D mutation is non-conservative and results in the loss of four polar contacts and the creation of three new polar interactions within the drug binding site; 6) the E796V mutation

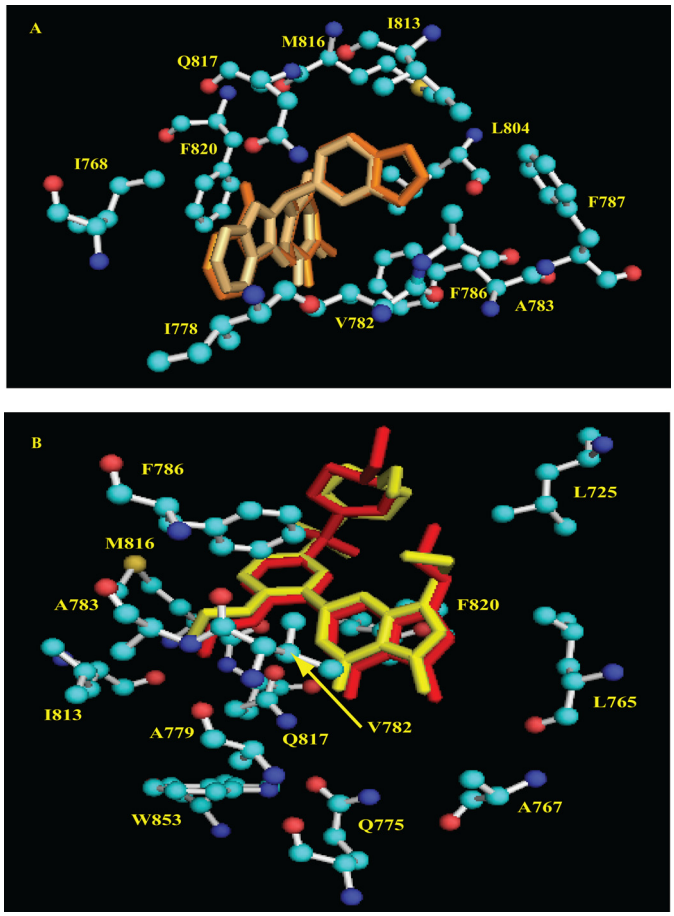

FIGURE 5. **Validation of the computer simulation of drug binding by comparison with the solved crystal structures of PDE5 catalytic domain complexed with either tadalafil or vardenafil.** *A*, shown is molecular simulation of tadalafil binding (*orange*) to the unliganded catalytic pocket of wild-type PDE5. The structure of tadalafil complexed with PDE5 in the crystal structure (PDB code 1XOZ) is shown in *light brown*. *Ball-and-stick structures* show the PDE5 drug binding residues for tadalafil from the crystal structure. A similar conformation of tadalafil is predicted by Autodock when performing a docking simulation of tadalafil to the crystal structure of the unliganded PDE5 catalytic domain (1T9R (33)). *B*, shown is *in silico* docking of vardenafil (*yellow*) to unliganded PDE5 compared with the solved crystal structure of vardenafil binding (*red*) to the catalytic domain (PDB code 1XP0 (25)). *Ball-and-stick structures* show the PDE5 binding determinants for vardenafil.

undergoes a dramatic loss of five polar contacts (two of which interact with water molecules in the binding pocket).

Performing *in silico* docking of tadalafil to the series of mutants we generated provided additional insight into the most important interaction sites of this drug with the binding pocket. Whereas the predicted conformation of tadalafil in the PDEm4 mutant (containing P773E, I778V, and E780L) was virtually indistinguishable from the wild-type conformation, the PDE5m5 (D803P, L804M, and N806D) mutant exhibited a substantial perturbation in predicted binding interactions (data not shown). The addition of three α-helix-14 (P773E, I778V, E780L) residues to generate PDE5m6 (P773E, I778V, E780L, D803P, L804M, N806D) resulted in a further perturbation of tadalafil conformation that is indistinguishable from the CD/m7 mutant (*i.e.* PDE5m6 plus four additional mutations: F787W, E796V, I813L, and S815K; data not shown).

We also generated a structural homology of the PDE6C catalytic domain and used Autodock to simulate the binding of

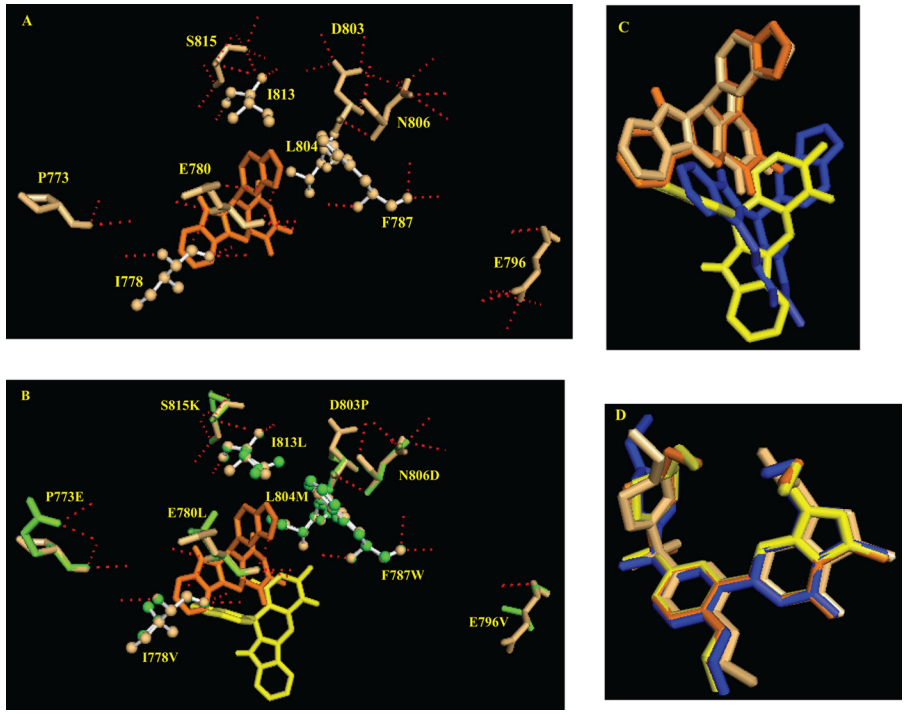

FIGURE 6. **Molecular simulation of tadalafil and vardenafil binding to the PDE5 catalytic domain.** *A*, the conformation of tadalafil (*orange*) docked to the catalytic domain of (PDB code 1XOZ) is shown with only the class-specific sites (*light brown*) within the binding pocket visualized. Residues displayed in *ball-and-stick format* are the four tadalafil interacting residues identified in the liganded crystal structure that are also class-specific sites. *Dashed lines* represent predicted polar interactions with neighboring atoms. *B*, shown is the same view as in *A*, with the substituted PDE6 residues (*green*) representing the homology model of the PDE5 CD/m7 mutant. Tadalafil is docked into the wild-type structure (*orange*) and the CD/m7 structure (*yellow*). *Dashed lines* represent predicted polar interactions with neighboring atoms. *C*, shown is a close-up comparison of the predicted docked conformations of tadalafil bound to PDE5 wild type (*orange*), CD/m7 (*yellow*), and a homology model of PDE6C (*blue*) compared with the crystal structure conformation (PDB code 1XOZ; *light brown*). *D*, shown are predicted conformations for vardenafil bound to the same catalytic domain structures as in *C*, except that vardenafil is docked to its corresponding PDE5 catalytic domain crystal structure (PDB code 1XP0) for the reference conformation (*light brown*).

tadalafil and vardenafil to the catalytic pocket. Fig. 6*C* shows that tadalafil is predicted to assume a very different orientation in the catalytic pocket of PDE6C. It is evident that the drug is unable to dock to the native, high affinity conformation observed for wild-type PDE5 (consistent with the pharmacological selectivity of tadalafil for PDE5 *versus* PDE6 (9)). In marked contrast to the tadalafil results, the docked structure for vardenafil assumed a similar conformation for the wild-type PDE5 catalytic domain, the CD/m7 mutant, and for the homology model of the PDE6C catalytic domain (Fig. 6*D*). The molecular simulation of vardenafil docking to the PDE5 and PDE6 homology models is consistent with the observation that of the 13 residues identified as contributing to vardenafil binding (25), evolutionary trace analysis identifies 10 of these residues as unanimous sites, with only 1 of the 13 being a PDE5/6 class-specific site.

In summary, molecular simulation of tadalafil and vardenafil binding to wild-type and mutant PDE5 catalytic domains support the conclusion that class-specific residues in the M-loop and its connecting α-helices account for the pharmacological selectivity of tadalafil for PDE5. These same amino acid residues when mutated have minor effects on vardenafil binding, consistent with previous studies that suggest that the so-called H-loop (aa 661–676; (27)) may be of greater importance for binding of sildenafil and vardenafil to the PDE5 catalytic domain (24, 33, 40).

Efforts to Determine Residues Critical for Catalytic Acceleration and Proper Expression of Recombinant Protein—Aside from previous identification of two mutations (A618G, A622G) in α-helix-6 of PDE5 that accelerate ~10-fold the rate of cGMP hydrolysis (11), the molecular basis for the 500-fold acceleration of catalytic activity of PDE6 compared with PDE5 is poorly understood. Using evolutionary trace and homology modeling, we identified A618G as well as two additional amino acids T621V and F686L as class-specific sites that we hypothesized could contribute to the greater turnover number of PDE6 compared with PDE5. We, therefore, created two full-length constructs, PDE5m1 (A618G, T621V, A622G) and PDE5m2 (A618G, T621V, A622G, F686L) that showed a 6.5- and 2-fold (respectively) increase in catalytic turnover number compared with the PDE5wt construct (Table 1). The k_{cat} value from PDE5m1 was consistent with the previous results from the PDE5/6 chimeric protein (11). However, the F686L change in PDE5m2 apparently negated the increased catalytic rate induced by the other mutated residues.

However, when we tested these same mutations using bacterial expression of the isolated catalytic domain, the recombinant proteins failed to exhibit enhanced catalytic efficiency; instead, a 4-fold decrease in activity was observed (supplemental Table S1). Adding additional class-specific mutations (V660T, S663L, I665Q, R667K; all within α-helix-8 of the H-loop) to the CD/m1 mutant resulted in a further reduction

in enzyme activity and decreased protein solubility (see CD/m1+H loop, supplemental Table S1).

PDE5 GAF domains may be required for effective or accurate protein folding of bacterially expressed site-directed mutants of PDE5 that target the H-loop or other structural elements immediately surrounding the metal ion binding sites. To test this, we generated constructs containing the PDE5 catalytic domain linked to the adjacent GAFb domain (aa 332–875) or to the tandem GAFa-GAFb domains (aa 81–875). Although we were able to maintain catalytic activity for the wild-type constructs, neither the GAFb/m1 nor the GAFab/m1 mutants showed any acceleration of catalytic activity (supplemental Table S1). We conclude that to study the structural basis for the 500-fold difference in catalytic turnover number for PDE5 and PDE6 will likely require expression of full-length recombinant protein in eukaryotic cells.

We were likewise unsuccessful in attempts to "reverse engineer" other groups of class-specific sites into full-length PDE5 or the isolated catalytic domain. As seen in supplemental Table S1, both of the full-length mutants PDE5m111 and PDE5m120 were expressed as predominantly insoluble proteins and lacking in hydrolytic activity. CD/m8 was generated by the addition of three class-specific sites (A823F, Q827F, and L828V) to the CD/m7 mutant (characterized above) rendering the expressed protein catalytically inactive even though reasonable amounts of soluble protein were purified. Unlike PDE5, which can be readily expressed in heterologous systems, it appears that several structural elements that are unique to the PDE6 catalytic domain need to be expressed in the native environment of the photoreceptor inner segment for proper folding of the catalytic domain to occur (18).

Conclusions—This study used evolutionary trace analysis to successfully identify amino acid residues responsible for selectivity of tadalafil binding to PDE5 *versus* PDE6. Substituting 10 class-specific sites in the M-loop region of the catalytic domain responsible for high affinity tadalafil binding to PDE5 lowered the drug binding affinity to a level approaching that of tadalafil for native cone PDE6 enzyme. This was accomplished without major perturbations of the binding affinity of vardenafil, demonstrating that other chemical classes of PDE5 inhibitors have different stabilizing interactions within the catalytic site. These results offer the potential for rational design of pharmacophores to enhance the selectivity of PDE5 inhibitors for their target enzyme and thereby reduce adverse side effects on PDE6 and the visual signaling pathway.

This paper also presents a comprehensive analysis of the evolution of vertebrate PDE5 and PDE6 enzyme families. Allowing evolutionary forces to conduct mutant screening to identify functionally important sites within the protein sequence of individual families revealed a high conservation of PDE5 residues in the regulatory half of the enzyme, (especially the GAFa domain and adjoining gap region before GAFb); this functional specialization may reflect the importance of allosteric regulation by cGMP binding that is transmitted to the enzyme active site. In contrast, the majority of conserved PDE6 residues occur within the GAFb domain, but the functional importance of this region remains to be elucidated.

In the absence of a successful system for producing large quantities of recombinant PDE6 for biochemical and structural studies, this approach of reverse-engineering individual PDE5 residues to their PDE6 counterparts is shown to be an effective strategy for understanding structure/function relationships for the PDE5 and PDE6 enzyme families. This work will increase our understanding of how genetic mutations in the PDE6 gene family result in retinal degenerative diseases as well as assist efforts to design the next generation of PDE5 inhibitors to better target diseases of the cardiovascular system.

Acknowledgments—We thank Hannah Gitschier and Elizabeth Dwinell for help with the cloning of several constructs used in this study and Dr. Xiujun Zhang for assistance with the drug inhibition experiments. Dr. Stacia Sower (University of New Hampshire) kindly provided Petromyzon marinus eyes for isolation of retinal tissue, Dr. Kelley Thomas and the staff of the UNH Hubbard Center for Genome Studies generously assisted in the analysis of genomic sequences that were used in this study, and Dr. Wayne Decatur (University of New Hampshire) provided guidance on protein visualization tools.

REFERENCES

1. Conti, M., and Beavo, J. (2007) Biochemistry and physiology of cyclic nucleotide phosphodiesterases. Essential components in cyclic nucleotide signaling. *Annu. Rev. Biochem.* **76,** 481–511
2. Cote, R. H. (2006) in *Cyclic Nucleotide Phosphodiesterases in Health and Disease* (Beavo, J. A., Francis, S. H., and Houslay, M. D., eds) pp. 165–193, CRC Press, Boca Raton, FL
3. Cote, R. H. (2004) Characteristics of photoreceptor PDE (PDE6). Similarities and differences to PDE5. *Int. J. Impot. Res.* **16,** S28–S33
4. Kameni Tcheudji, J. F., Lebeau, L., Virmaux, N., Maftei, C. G., Cote, R. H., Lugnier, C., and Schultz, P. (2001) Molecular organization of bovine rod cGMP-phosphodiesterase 6. *J. Mol. Biol.* **310,** 781–791
5. Kajimura, N., Yamazaki, M., Morikawa, K., Yamazaki, A., and Mayanagi, K. (2002) Three-dimensional structure of non-activated cGMP phosphodiesterase 6 and comparison of its image with those of activated forms. *J. Struct. Biol.* **139,** 27–38
6. Goc, A., Chami, M., Lodowski, D. T., Bosshart, P., Moiseenkova-Bell, V., Baehr, W., Engel, A., and Palczewski, K. (2010) Structural characterization of the rod cGMP phosphodiesterase 6. *J. Mol. Biol.* **401,** 363–373
7. Gillespie, P. G., and Beavo, J. A. (1989) Inhibition and stimulation of photoreceptor phosphodiesterases by dipyridamole and M&B 22,948. *Mol. Pharmacol.* **36,** 773–781
8. D'Amours, M. R., Granovsky, A. E., Artemyev, N. O., and Cote, R. H. (1999) Potency and mechanism of action of E4021, a type 5 phosphodiesterase isozyme-selective inhibitor, on the photoreceptor phosphodiesterase depend on the state of activation of the enzyme. *Mol. Pharmacol.* **55,** 508–514
9. Zhang, X., Feng, Q., and Cote, R. H. (2005) Efficacy and selectivity of phosphodiesterase-targeted drugs in inhibiting photoreceptor phosphodiesterase (PDE6) in retinal photoreceptors. *Invest. Ophthalmol. Vis. Sci.* **46,** 3060–3066
10. Laties, A., and Sharlip, I. (2006) Ocular safety in patients using sildenafil citrate therapy for erectile dysfunction. *J. Sex. Med.* **3,** 12–27
11. Granovsky, A. E., and Artemyev, N. O. (2001) Partial reconstitution of photoreceptor cGMP phosphodiesterase characteristics in cGMP phosphodiesterase-5. *J. Biol. Chem.* **276,** 21698–21703
12. Zoraghi, R., Francis, S. H., and Corbin, J. D. (2007) Critical amino acids in phosphodiesterase-5 catalytic site that provide for high affinity interaction with cyclic guanosine monophosphate and inhibitors. *Biochemistry* **46,** 13554–13563
13. Granovsky, A. E., Natochin, M., McEntaffer, R. L., Haik, T. L., Francis, S. H., Corbin, J. D., and Artemyev, N. O. (1998) Probing domain functions of chimeric PDE6α′/PDE5 cGMP-phosphodiesterase. *J. Biol. Chem.* **273,**

24485–24490
14. Piriev, N. I., Yamashita, C. K., Shih, J., and Farber, D. B. (2003) Expression of cone photoreceptor cGMP-phosphodiesterase α' subunit in Chinese hamster ovary, 293 human embryonic kidney, and Y79 retinoblastoma cells. *Mol. Vis.* **9,** 80–86
15. White, J. B., Thompson, W. J., and Pittler, S. J. (2004) Characterization of 3′,5′ cyclic nucleotide phosphodiesterase activity in Y79 retinoblastoma cells. Absence of functional PDE6. *Mol. Vis.* **10,** 738–749
16. Zhang, J., Kuvelkar, R., Wu, P., Egan, R. W., Billah, M. M., and Wang, P. (2004) Differential inhibitor sensitivity between human recombinant and native photoreceptor cGMP-phosphodiesterases (PDE6s). *Biochem. Pharmacol.* **68,** 867–873
17. Muradov, H., Boyd, K. K., and Artemyev, N. O. (2006) Analysis of PDE6 function using chimeric PDE5/6 catalytic domains. *Vision Res.* **46,** 860–868
18. Muradov, H., Boyd, K. K., Haeri, M., Kerov, V., Knox, B. E., and Artemyev, N. O. (2009) Characterization of human cone phosphodiesterase-6 ectopically expressed in *Xenopus laevis* rods. *J. Biol. Chem.* **284,** 32662–32669
19. Francis, S. H., Zoraghi, R., Kotera, J., Ke, H., Bessay, E. P., Blount, M. A., and Corbin, J. D. (2006) in *Cyclic Nucleotide Phosphodiesterases in Health and Disease* (Beavo, J. A., Francis, S. H., and Houslay, M. D., eds) pp. 131–164, CRC Press, Boca Raton, FL
20. Bischoff, E. (2004) Potency, selectivity, and consequences of nonselectivity of PDE inhibition. *Int. J. Impot. Res.* **16,** S11–S14
21. Kerr, N. M., and Danesh-Meyer, H. V. (2009) Phosphodiesterase inhibitors and the eye. *Clin. Experiment Ophthalmol.* **37,** 514–523
22. Laties, A. M. (2009) Vision disorders and phosphodiesterase type 5 inhibitors. A review of the evidence to date. *Drug Safety* **32,** 1–18
23. Supuran, C. T., Mastrolorenzo, A., Barbaro, G., and Scozzafava, A. (2006) Phosphodiesterase 5 inhibitors. Drug design and differentiation based on selectivity, pharmacokinetic, and efficacy profiles. *Curr. Pharm. Des.* **12,** 3459–3465
24. Chen, G., Wang, H., Robinson, H., Cai, J., Wan, Y., and Ke, H. (2008) An insight into the pharmacophores of phosphodiesterase-5 inhibitors from synthetic and crystal structural studies. *Biochem. Pharmacol.* **75,** 1717–1728
25. Card, G. L., England, B. P., Suzuki, Y., Fong, D., Powell, B., Lee, B., Luu, C., Tabrizizad, M., Gillette, S., Ibrahim, P. N., Artis, D. R., Bollag, G., Milburn, M. V., Kim, S. H., Schlessinger, J., and Zhang, K. Y. (2004) Structural basis for the activity of drugs that inhibit phosphodiesterases. *Structure* **12,** 2233–2247
26. Sung, B. J., Hwang, K. Y., Jeon, Y. H., Lee, J. I., Heo, Y. S., Kim, J. H., Moon, J., Yoon, J. M., Hyun, Y. L., Kim, E., Eum, S. J., Park, S. Y., Lee, J. O., Lee, T. G., Ro, S., and Cho, J. M. (2003) Structure of the catalytic domain of human phosphodiesterase 5 with bound drug molecules. *Nature* **425,** 98–102
27. Huai, Q., Liu, Y., Francis, S. H., Corbin, J. D., and Ke, H. (2004) Crystal structures of phosphodiesterases 4 and 5 in complex with inhibitor 3-isobutyl-1-methylxanthine suggest a conformation determinant of inhibitor selectivity. *J. Biol. Chem.* **279,** 13095–13101
28. Wang, H., Ye, M., Robinson, H., Francis, S. H., and Ke, H. (2008) Conformational variations of both phosphodiesterase-5 and inhibitors provide the structural basis for the physiological effects of vardenafil and sildenafil. *Mol. Pharmacol.* **73,** 104–110
29. Carleton, K. L., Spady, T. C., and Cote, R. H. (2005) Rod and cone opsin families differ in spectral tuning domains but not signal transducing domains as judged by saturated evolutionary trace analysis. *J. Mol. Evol.* **61,** 75–89
30. Lichtarge, O., and Wilkins, A. (2010) Evolution. A guide to perturb protein function and networks. *Curr. Opin. Struct. Biol.* **20,** 351–359
31. Swofford, D. L. (2000) *PAUP*. Phylogenetic Analysis Using Parsimony and Other Methods*, Sinauer Associates, Sunderland, MA
32. Schwede, T., Kopp, J., Guex, N., and Peitsch, M. C. (2003) SWISS-MODEL. An automated protein homology-modeling server. *Nucleic Acids Res.* **31,** 3381–3385
33. Zhang, K. Y., Card, G. L., Suzuki, Y., Artis, D. R., Fong, D., Gillette, S., Hsieh, D., Neiman, J., West, B. L., Zhang, C., Milburn, M. V., Kim, S. H., Schlessinger, J., and Bollag, G. (2004) A glutamine switch mechanism for nucleotide selectivity by phosphodiesterases. *Mol. Cell* **15,** 279–286
34. Laskowski, R. A., MacArthur, M. W., Moss, D. S., and Thornton, J. M. (1993) PROCHECK: a program to check the stereochemical quality of protein structures. *J. Appl. Crystallogr.* **26,** 283–291
35. Blount, M. A., Beasley, A., Zoraghi, R., Sekhar, K. R., Bessay, E. P., Francis, S. H., and Corbin, J. D. (2004) Binding of tritiated sildenafil, tadalafil, or vardenafil to the phosphodiesterase-5 catalytic site displays potency, specificity, heterogeneity, and cGMP stimulation. *Mol. Pharmacol.* **66,** 144–152
36. Rybalkin, S. D., Rybalkina, I. G., Shimizu-Albergine, M., Tang, X. B., and Beavo, J. A. (2003) PDE5 is converted to an activated state upon cGMP binding to the GAF A domain. *EMBO J.* **22,** 469–478
37. Bradford, M. M. (1976) A rapid and sensitive method for the quantitation of microgram quantities of protein utilizing the principle of protein-dye binding. *Anal. Biochem.* **72,** 248–254
38. Cote, R. H. (2000) Kinetics and regulation of cGMP binding to noncatalytic binding sites on photoreceptor phosphodiesterase. *Methods Enzymol.* **315,** 646–672
39. Trott, O., and Olson, A. J. (2010) AutoDock Vina. Improving the speed and accuracy of docking with a new scoring function, efficient optimization, and multithreading. *J. Comput. Chem.* **31,** 455–461
40. Wang, H., Liu, Y., Huai, Q., Cai, J., Zoraghi, R., Francis, S. H., Corbin, J. D., Robinson, H., Xin, Z., Lin, G., and Ke, H. (2006) Multiple conformations of phosphodiesterase-5. Implications for enzyme function and drug development. *J. Biol. Chem.* **281,** 21469–21479
41. Francis, S. H., Sekhar, K. R., Ke, H., and Corbin, J. D. (2011) Inhibition of cyclic nucleotide phosphodiesterases by methylxanthines and related compounds. *Handb. Exp. Pharmacol.* **200,** 93–133